# MedGA: A novel evolutionary method for image enhancement in medical imaging systems

Leonardo Rundo [a,b,1], Andrea Tangherloni [a,1], Marco S. Nobile [a,c], Carmelo Militello [b], Daniela Besozzi [a], Giancarlo Mauri [a,c], Paolo Cazzaniga [d,c,*]

[a] University of Milano-Bicocca, Department of Informatics, Systems and Communication, Milano 20126, Italy
[b] Institute of Molecular Bioimaging and Physiology, Italian National Research Council, Cefalú (PA) 90015, Italy
[c] SYSBIO.IT Centre of Systems Biology, Milano 20126, Italy
[d] University of Bergamo, Department of Human and Social Sciences, Bergamo 24129, Italy

## ARTICLE INFO

## ABSTRACT

Medical imaging systems often require the application of image enhancement techniques to help physicians in anomaly/abnormality detection and diagnosis, as well as to improve the quality of images that undergo automated image processing. In this work we introduce MedGA, a novel image enhancement method based on Genetic Algorithms that is able to improve the appearance and the visual quality of images characterized by a bimodal gray level intensity histogram, by strengthening their two underlying sub-distributions. MedGA can be exploited as a pre-processing step for the enhancement of images with a nearly bimodal histogram distribution, to improve the results achieved by downstream image processing techniques. As a case study, we use MedGA as a clinical expert system for contrast-enhanced Magnetic Resonance image analysis, considering Magnetic Resonance guided Focused Ultrasound Surgery for uterine fibroids. The performances of MedGA are quantitatively evaluated by means of various image enhancement metrics, and compared against the conventional state-of-the-art image enhancement techniques, namely, histogram equalization, bi-histogram equalization, encoding and decoding Gamma transformations, and sigmoid transformations. We show that MedGA considerably outperforms the other approaches in terms of signal and perceived image quality, while preserving the input mean brightness. MedGA may have a significant impact in real healthcare environments, representing an intelligent solution for Clinical Decision Support Systems in radiology practice for image enhancement, to visually assist physicians during their interactive decision-making tasks, as well as for the improvement of downstream automated processing pipelines in clinically useful measurements.

© 2018 Elsevier Ltd. All rights reserved.

## 1. Introduction

Nowadays, medical imaging systems play a key role in the clinical workflow, thanks to their capability of representing anatomical and physiological features that are otherwise inaccessible to inspection, thus proposing accurate imaging biomarkers and clinically useful information (Lambin et al., 2017; Rueckert, Glocker, & Kainz, 2016). Medical images are considerably different from the pictures usually analyzed in Pattern Recognition and Computer Vision, as regards the appearance of the depicted objects as well as the information conveyed by the pixels. As a matter of fact, medical imaging techniques exploit several different principles to measure spatial distributions of physical attributes of the human body, allowing us to better understand complex or rare diseases (Toennies, 2017). The effectiveness of such techniques can be reduced by a plethora of phenomena, such as noise and partial volume effects (Toennies, 2017), which might affect the measurement processes involved in imaging and data acquisition devices. In addition, computer-aided medical image acquisition procedures generally include reconstruction methods (producing two, three, or even four dimensional imaging data), which could cause the appearance of artifacts. Image contrast and details might also be impaired by the procedures used in medical imaging, as well as by the physiological nature of the body part under investigation.

---

* Corresponding author at: University of Bergamo, Department of Human and Social Sciences, Bergamo 24129, Italy

*E-mail addresses:* leonardo.rundo@disco.unimib.it (L. Rundo), andrea.tangherloni @disco.unimib.it (A. Tangherloni), marco.nobile@disco.unimib.it (M.S. Nobile), carmelo.militello@ibfm.cnr.it (C. Militello), daniela.besozzi@unimib.it (D. Besozzi), mauri@disco.unimib.it (G. Mauri), paolo.cazzaniga@unibg.it (P. Cazzaniga).

[1] These authors contributed equally.

Medical images actually convey an amount of information—mainly related to high image resolution and high pixel depth—that could overwhelm the human vision capabilities in distinguishing among dozens of gray levels (Ortiz, Górriz, Ramírez, Salas-Gonzalez, & Llamas-Elvira, 2013). Improving the appearance—and the visual quality—of medical images is therefore essential to provide physicians with valuable information that would not be immediately observable in the original image, assisting them in anomaly detection, diagnosis and treatment. This kind of diagnosis includes two basic processes: image observation (visual perception), and diagnostic interpretation (cognition) (Krupinski, 2010). Errors occurring in these diagnostic and therapeutic decision-making processes may have a significant impact on patient care, most notably possible misdiagnoses. In this context, image enhancement techniques aim at realizing a specific improvement in the quality of a given medical image. The enhanced image is expected to better reveal certain features, compared to their original appearance (de Araujo, Constantinou, & Tavares, 2014). In particular, these methods could have a significant clinical impact when the dynamic range of the actual pictorial content is not commensurable with the range of the displayed data (i.e., monitor luminance response), as well as when the input image is characterized either by a high level of noise or by a low contrast (Gonzalez & Woods, 2002; Paranjape, 2009). This also applies to specialized computer screens for diagnostic reporting.

Although the majority of the enhancement techniques are typically applied to generate improved images for a human observer, others are exploited as a pre-processing step to provide enhanced images to further algorithms for computer-assisted analyses (Paranjape, 2009). The first category includes techniques devoted to remove noise, enhance contrast and sharpen the details. The second category, partially overlapped with the former one, includes additional techniques such as edge detection and object segmentation for automated processing (Rangayyan, 2009). It was shown that a high-contrast medical image could lead to a better interpretation of the different adjacent tissues in the imaged body part (Chen et al., 2015). Accordingly, the resulting enhanced image—in terms of signal intensities of different tissues—can facilitate the automated segmentation, feature extraction, and classification of these tissues.

In the clinical routine, Contrast-Enhanced (CE) Magnetic Resonance Imaging (MRI) is a diagnostic technique that enables a more precise assessment of the imaged tissues after the administration of a Gadolinium-based contrast medium in patients (Sourbron & Buckley, 2013). MRI is currently the most prominent modality to obtain soft-tissue imaging (Brown, Cheng, Haacke, Thompson, & Venkatesan, 2014), especially in oncology, since it provides significant improvements—in terms of image contrast and resolution—between lesion and healthy tissue (Metcalfe et al., 2013). For these reasons, MRI is considered more suitable than Computed Tomography in determining the extent of cancer infiltration. Furthermore, the excellent MRI soft-tissue contrast has led to an increasing role of this modality in target volume delineation for therapy applications, such as image-guided surgery and radiotherapy treatment, and for patients follow-up (i.e., staging and assessing tumor response) (Evans, 2008). However, MRI data are affected by acquisition noise (Styner, Brechbuhler, Széckely, & Gerig, 2000) and are also prone to imaging artifacts, related to magnetic susceptibility and large intensity inhomogeneities of the static magnetic field (i.e., streaking or shadowing artifacts (Bellon et al., 1986)), especially using high magnetic field strengths. These aspects make MR image enhancement a challenging task aiming at improving the results of automatic segmentation methods. The existing image enhancement approaches generally attempt to improve the contrast level of the whole image and do not address the issues related to overlapped gray level intensities; as a consequence, neither the region contour sharpness nor the image thresholding results can be improved. In the case of threshold-based image segmentation with two classes (i.e., foreground and background) (Muangkote, Sunat, & Chiewchanwattana, 2017), the input image is assumed to have a bimodal distribution of the histogram bins (Xue & Zhang, 2012). Thus, an appropriate image enhancement method that yields medical images with a sharper bimodal distribution is required. However, determining the best pre-processing of an image—able to preserve the structural information of the image, while enhancing the underlying bimodal distribution—is a complex task on a multimodal fitness landscape that demands the use of global optimization approaches.

This paper presents a novel image enhancement technique based on Genetic Algorithms (GAs) (Holland, 1992), called MedGA, specifically aimed at strengthening the sub-distributions in medical images with an underlying bimodal histogram of the gray level intensities. Among the existing soft computing methods for global optimization, GAs represent the most suitable technique for this application, because of the discrete structure of the candidate solutions and the intrinsic combinatorial structure of the problem under investigation.

In this work, we apply MedGA to a clinical context involving CE MR image analysis, i.e., Magnetic Resonance guided Focused Ultrasound Surgery (MRgFUS) for uterine fibroids. The performances of MedGA are quantitatively evaluated by means of the most relevant image enhancement metrics, and compared against the conventional state-of-the-art image enhancement techniques, namely, histogram equalization, bi-histogram equalization, encoding and decoding Gamma transformations, and three instances of sigmoid transformation. Considering the possible clinical applications, MedGA is able to improve the visual perception of a Region of Interest (ROI) in MRI data with an underlying bimodal intensity distribution. In addition, MedGA can be used as an intelligent pre-processing step, in red any pipeline defined to realize an efficient threshold-based image segmentation with two classes (i.e., binarization), applied to expert systems working on MRI data. Indeed, image thresholding approaches performed on CE MR image regions could considerably benefit from input data pre-processed by MedGA.

The main contributions of MedGA in the context of expert and intelligent clinical systems can be briefly outlined as follows. MedGA acts as an expert system by playing a two-fold role: (*i*) image enhancement to visually assist physicians during their interactive decision-making tasks, and (*ii*) improvement of the results in downstream automated processing pipelines for clinically useful measurements. The rationale behind the development of MedGA is the need of an intelligent model that is well-suited to effectively enhance medical images with roughly bimodal histograms. To the best of our knowledge, MedGA is the first work that explicitly deals with the improvement of thresholding-based segmentation results (Xue & Zhang, 2012). Therefore, our computational framework can be employed as an intelligent solution in Clinical Decision Support Systems (CDSSs). As a matter of fact, MedGA represents an interpretable computational model (Castelvecchi, 2016) that allows for the understandability of the results (i.e., the gray level histogram is readable by the user). The compelling issues related to the interpretability of Machine Learning and Computational Intelligence methods in medicine are fundamental for the adoption and the clinical feasibility of a novel CDSS (Cabitza, Rasoini, & Gensini, 2017). In addition, no user interaction is required thanks to a reliable calibration step for the parameter settings of the GA. The goal of this paper consists in showing that evolutionary computation methods can boost the state-of-the-art performance in medical image enhancement, thus fostering GAs as a new concrete support tool for the clinical practice. Such an expert system may have a significant impact in real healthcare environments.

This manuscript is organized as follows. Related literature works and a theoretical comparison with existing methods are outlined in Section 2. Section 3 describes the MedGA image enhancement method. The evaluation metrics and the MR images used to assess the performance of MedGA are described in Section 4. Section 5 presents the achieved experimental results, by extensively explaining parameter analysis of MedGA. Finally, discussions and conclusive remarks are reported in Sections 6 and 7, respectively.

## 2. Background

### 2.1. Related work

Most of the existing enhancement techniques are empirical or heuristic methods—strongly related to a particular type of images—that generally aim at improving the contrast level of images degraded during the acquisition process (Chen, Yu, Tian, Chen, & Zhou, 2018). As a matter of fact, finding the best gray level mapping that adaptively enhances each different input image can be considered an optimization problem (Draa & Bouaziz, 2014; Paulinas & Ušinskas, 2007). Unfortunately, no unifying theory employing a standardized image quality measure is currently available to define a general criterion for image enhancement (Munteanu & Rosa, 2004). In addition, in the case of medical imaging, techniques tailored on specific tasks are necessary to achieve a significant enhancement and, in general, interactive procedures involving considerable human effort are needed to obtain satisfactory results.

In order to achieve objective and reproducible measurements conveying clinically useful information, operator-dependence should be minimized by means of automated methods. Pointwise operations in the spatial (pixel) domain, representing the simplest form of image processing, are effective solutions since efficiency requirements have also to be met. In the case of image enhancement, they re-map each input gray level into a certain output gray level, according to a global transformation (Gonzalez & Woods, 2002). Thus, such kind of techniques treat images as a whole, without considering specific features of different regions, or selectively distinguishing between a collection of contrast enhancement degrees or settings (Munteanu & Rosa, 2004). Histogram Equalization (HE) is the most common global image enhancement technique, whose aim is to uniformly redistribute the input gray level values according to the cumulative density function of its histogram (Gonzalez & Woods, 2002; Hall, 1974). Unfortunately, HE does not take into account the image mean intensity (Chen & Ramli, 2003), which is subject to a significant change during the equalization process by invariably shifting the output mean brightness to the middle gray level, regardless of the mean gray level in the input image (Gan et al., 2014). Consequently, HE is not able to preserve the input mean brightness, possibly suffering from over-enhancement, and giving rise to artifacts such as the so-called washed-out effect (Chen & Ramli, 2003). This global transformation method applies contrast stretching just on gray levels with the highest frequencies, causing a significant contrast loss concerning the gray levels characterized by low frequencies in the input histogram (Kim, 1997). Bi-Histogram Equalization (Bi-HE), which is a refined version of the traditional HE, was proposed to overcome the limitations related to input mean brightness preservation, mainly caused by histogram flattening (Kim, 1997). Firstly, Bi-HE splits the original histogram into two sub-histograms according to the global mean of the original image; afterwards, the sub-histograms are independently processed by applying the standard HE method to each of them.

The complexity of the enhancement criteria to be met (i.e.,

the effective contrast stretching combined with image detail preserving) leads to the application of global search meta-heuristics that allow for coping with several constraints, which are not generally tractable by means of traditional exhaustive computational approaches (Munteanu & Rosa, 2004; Ortiz et al., 2013; Paulinas & Ušinskas, 2007). Evolutionary methods have been widely adopted in the image enhancement domain to find the optimal enhancement kernel (Munteanu & Rosa, 2004), sequence of filters (Kohmura & Wakahara, 2006), or input-output mapping transformation (Carbonaro & Zingaretti, 1999; Saitoh, 1999). Recently, Hashemi, Kiani, Noroozi, and Moghaddam (2010) proposed a GA-based method that efficiently encodes the histogram by means of the non-zero intensity levels, by employing genetic operators that directly process images to increase the visible details and contrast of low illumination regions, especially in the case of high dynamic ranges. The authors argued that this method yields "natural-looking" images, considering the visual appearance.

Regarding other evolutionary computation approaches, Genetic Programming (GP) (Koza, 1992) was shown to be a powerful framework to select and combine existing algorithms in the most suitable way. Differently to GAs, GP evolves a population of functions, or more generally, computer programs to solve a computational task. The solutions in the computer program space can be represented as trees, lines of code, expressions in prefix or postfix notations as well as strings of variable length (Castelli, Vanneschi, & Silva, 2014). For instance, Bianco, Ciocca, and Schettini (2017) tackled the video change detection problem (among the frames of video streams) by combining existing algorithms *via* different GP solutions exploiting several fusion schemes. The fitness function was composed of different performance measures regarding change detection evaluation. For what concerns the application of GP in image enhancement, Poli and Cagnoni (1997) proposed an approach to yield optimally pseudo-colored images for visualization purposes, aiming at combining multiple gray-scale images (e.g., time-varying images, multi-modal medical images, and multi-band satellite images) into a single pseudo-color image. This approach relies on user interactions to determine which candidate solution should be the winner in tournament selection, so it does not explicitly require a fitness function. As case studies, a pair of brain MRI sequences were fused as well as the motion of the heart on echocardiographic images was synthesized into a single pseudo-color image.

Other works exploited Swarm Intelligence techniques. The approach presented in Shanmugavadivu and Balasubramanian (2014), called Multi-Objective Histogram Equalization, uses Particle Swarm Optimization (Kennedy & Eberhart, 1995) to enhance the contrast and preserve the brightness at the same time. Draa and Bouaziz (2014) employed the same encoding of candidate solutions and histogram mapping strategy described in Hashemi et al. (2010), within an optimization strategy based on the Artificial Bee Colony (ABC) algorithm (Karaboga & Basturk, 2007). However, since ABC natively works in a continuous space, while a discrete representation is used for the solutions (i.e., gray-level mapping), a discretization step is mandatory in the correction operation during the search phase. An alternative approach using the ABC algorithm for image contrast enhancement was proposed in Chen et al. (2018), wherein the optimal values for the parameters of a parametric image transformation, namely the Incomplete Beta Function, are estimated. Differently to the work described in Draa and Bouaziz (2014), the optimization procedure is carried out in a continuous search space. Finally, multi-objective Bat Optimization and a neuron-based model of Dynamic Stochastic Resonance were combined in Singh, Verma, and Sharma (2017) for the enhancement of brain MR images.
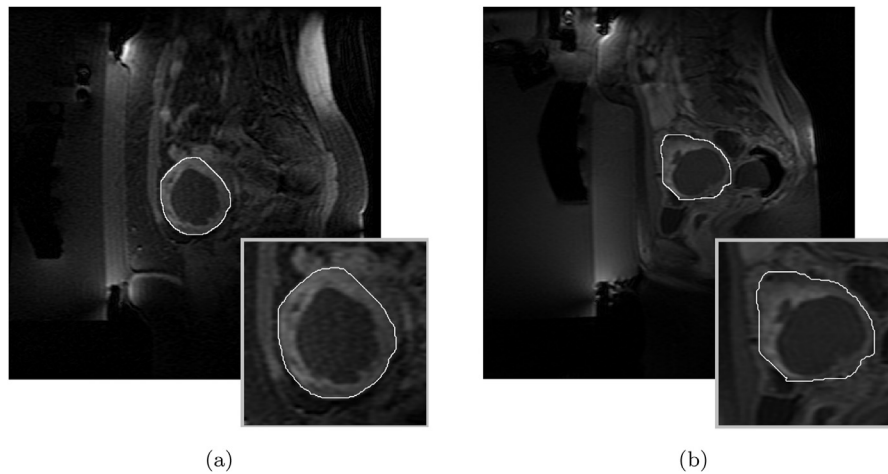
(a)                                                    (b)

**Fig. 1.** Examples of MR images. The ROI bounding region (i.e., the delineated uterus region), which includes the actual ROI (i.e., the uterine fibroid region), is highlighted with a white contour. The image regions including the ROIs, zoomed at the bottom right of each sub-figure, are characterized by nearly bimodal histograms.

## 2.2. Theoretical comparison with existing methods

It is worth noting that all works mentioned in Section 2.1 are focused on consumer electronics or medical applications, to obtain more "visually pleasant" images by mainly increasing the contrast of the whole image. On the contrary, the main key novelty of MedGA consists in better revealing the two underlying sub-distributions occurring in an image sub-region characterized by a roughly bimodal histogram, overcoming the limitations of the state-of-the-art contrast enhancement methods, which could produce false edges and consequently over-segmentation when the input images are affected by noise, as in the case of MRI data (Gandhamal, Talbar, Gajre, Hani, & Kumar, 2017). There exist other algorithms, like Histogram Specification (HS), whose aim is similar to MedGA and consists in matching the histogram of the gray level intensities of the input MR image with a desired output histogram (Gonzalez & Woods, 2002). Unfortunately, this approach cannot be applied to process image datasets characterized by a high variability in gray level distributions, since the histogram to be matched should be defined either *a priori* for the whole dataset, or interactively for each processed image, through a procedure that consists in strengthening and shaping the two underlying sub-distributions. In such cases, to automatically identify the best solution it is more advantageous to employ global search meta-heuristics, like GAs used in MedGA.

Even though MedGA exploits the same encoding of candidate solutions defined in Hashemi et al. (2010) and Draa and Bouaziz (2014), its purpose is very different since it was designed to explicitly strengthen the two sub-distributions of medical images characterized by an underlying bimodal histogram. To this aim, we defined a specific fitness function that emphasizes the two Gaussian distributions composing a bimodal histogram. This achievement plays a fundamental role for threshold-based segmentation approaches, since they strongly rely on the assumption that the bimodal histogram under investigation is composed of two nearly Gaussian distributions with almost equal size and variance (Xue & Zhang, 2012).

MedGA also differs from GP-based approaches whose generated solutions might have a large size (Castelli et al., 2014), even when the GP model is implemented efficiently, thus representing a limitation that could significantly impair the readability and interpretability of the final outcome. Moreover, MedGA does not require any user interaction step, differently to Poli and Cagnoni (1997) where the user, being directly involved in the tournament selection, controls the evolution of simple programs that

enhance and integrate multiple gray-scale images into a single pseudo-color image.

## 3. MedGA: An intelligent method based on Genetic Algorithms for medical image enhancement

MedGA is a global enhancement technique able to improve the details of medical images characterized by an underlying bimodal histogram of gray levels. Given a medical image wherein a ROI needs to be enhanced to achieve further analyses, MedGA aims at improving the ROI quality to facilitate the classification among different neighboring tissues, in order to support both the interpretation tasks by experienced radiologists and automated image analysis approaches.

The image enhancement carried out by MedGA focuses on the pixels within a sub-region of the input MRI, called ROI bounding region, including the ROI itself. To be more precise, starting from an MR image (Fig. 1), a bounding region that roughly includes the actual ROI (e.g., the uterus region including uterine fibroids in Fig. 1) is identified by using either a manual or a computational method. Afterwards, the entire original MR image is cropped at the smallest rectangular box including the previously identified ROI bounding region. The pixels included in the rectangular cropped image, but external to the ROI bounding region, are set to zero (i.e., the black level). So doing, an image characterized by a nearly bimodal histogram is obtained. Then, a linear contrast stretching is applied to the initial full range of gray levels, that is, the ordered set $\mathcal{L}_{in} = [l_{in}^{(min)}, l_{in}^{(min)} + 1, \ldots, l_{in}^{(max)} - 1, l_{in}^{(max)}] \subset \mathbb{N}$, where $l \neq l'$ for any $l, l' \in \mathcal{L}_{in}$. The integers $l_{in}^{(min)}$ and $l_{in}^{(max)}$ in $\mathcal{L}_{in}$ denote the minimum and maximum non-zero gray levels of the analyzed image sub-region, respectively. The linear contrast stretching applied to $\mathcal{L}_{in}$ exploits the extended range of the non-zero gray levels, that is, the ordered set $\mathcal{L}'_{in} = [1, \ldots, l_{in}^{(max)}] \subset \mathbb{N}$, where, typically, $l_{in}^{(min)} > 1$. Note that the zero-padding pixels (i.e., the pixels corresponding to the level 0) are not taken into account, and that any element of $\mathcal{L}_{in}$ is also an element of $\mathcal{L}'_{in}$. This normalization operation, which employs only values of gray levels already representable in the initial dynamic range, does not alter the image content and allows MedGA to process additional intensity levels with respect to the initial full range $\mathcal{L}_{in}$, by considering the intensity variability within the analyzed MRI dataset. It is worth noting that the pre-processing described hereby does not exploit any method that could affect the actual pictorial content (e.g., spatial or frequency filtering).
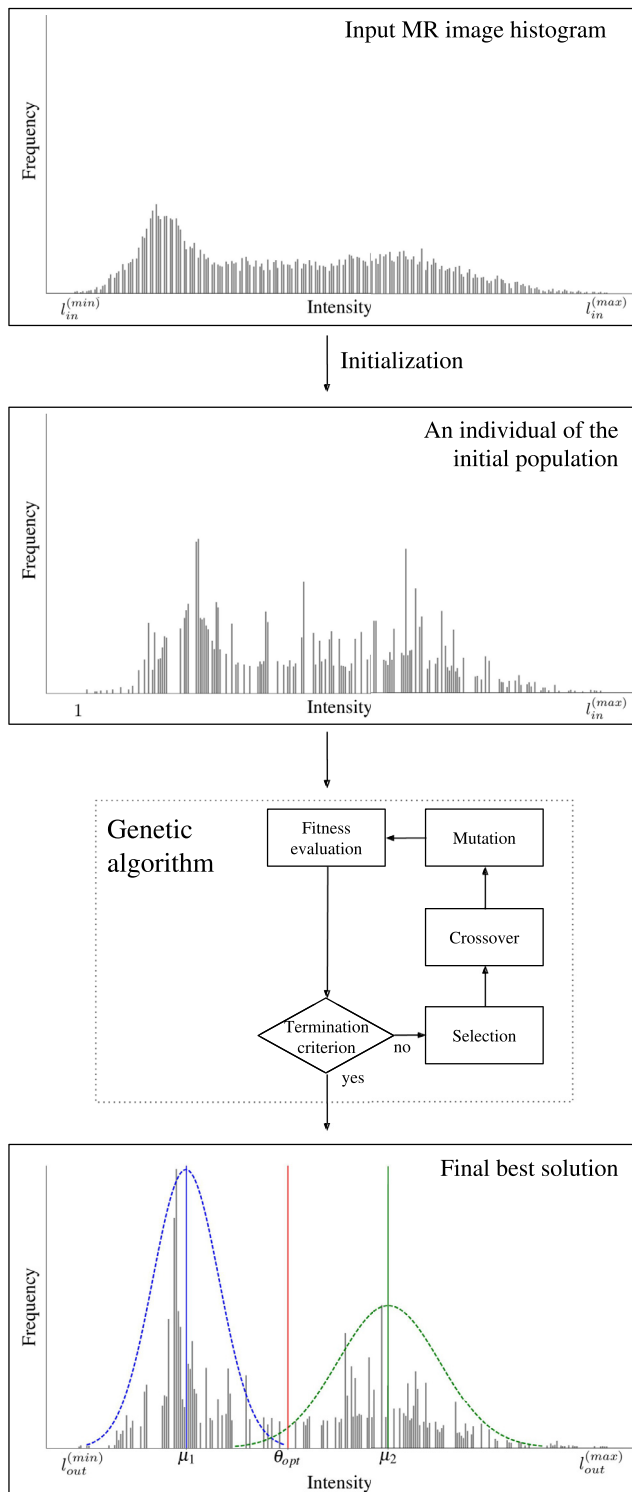
**Fig. 2.** Workflow of MedGA: the individuals are initialized according to the characteristics of the input MR image, and processed by the GA. The final best solution of MedGA strengthens the two underlying distributions in the gray levels intensity characterized by mean values $\mu_1$ and $\mu_2$ and standard deviations $\sigma_1$ and $\sigma_2$, respectively. The two distributions are highlighted in the plot with blue and green dashed lines. (For interpretation of the references to color in this figure legend, the reader is referred to the web version of this article.)

MedGA exploits a population $P$ of individuals $C_i = [C_i(1), C_i(2), \ldots, C_i(n)]$ (with $i = 1, \ldots, |P|$) defined as circular arrays of integer numbers of size $n$, where $n = |\mathcal{L}'_{in}|$ corresponds to the number of different gray levels belonging to $\mathcal{L}'_{in}$ identified in the input MR image (i.e., the gray levels whose frequency is greater than zero in the input MR image). Each individual $C_i \in P$ is randomly initialized by sampling $n$ integer values from the discrete uniform distribution in $\mathcal{L}'_{in}$. The $n$ values are then sorted in ascending order so that the intensity levels $C_i(j)$ (with $j = 1, \ldots, n$) codified by the individual can be mapped to the intensity levels of the input MR image (i.e., the gray level frequencies of the input MR image are assigned to the corresponding intensity levels of the individual). During the initialization of the individuals, if an integer value is sampled more than once then the frequency values of the input MR image, corresponding to these gray level intensities, are summed up and assigned to the same gray level of the individual.

The rationale of MedGA is to process the ordered set $\mathcal{L}'_{in}$ by modifying its gray levels using a sequence of genetic operators, to obtain a solution characterized by a stronger bimodal gray level distribution in an output gray-scale range $\mathcal{L}_{out} = [l_{out}^{(min)}, \ldots, l_{out}^{(max)}] \subset \mathbb{N}$, where any element of $\mathcal{L}_{out}$ is also an element of $\mathcal{L}'_{in}$. In such a way, a direct mapping between the gray levels of the original image and the final one is defined, so that each gray level in the original histogram is replaced with the gray level value contained by the same position in the final best solution $C_{best} \in P$. MedGA realizes this global intensity transformation by improving the separation between $\mathcal{H}_{1,i}$ and $\mathcal{H}_{2,i}$, which represent the dark and bright sub-regions of the histogram $\mathcal{H}_i$ encoded by the individual $C_i$, respectively. To this aim, MedGA exploits the optimal threshold $\theta_{opt, i}$ adaptively selected using the Iterative Optimal Threshold Selection (IOTS) method (Ridler & Calvard, 1978; Trussell, 1979). This procedure yields enhanced medical images that better reveal the bimodal intensity distribution in computer-assisted ROI extraction tasks.

At each iteration of MedGA, a number of individuals properly selected from the current population are inserted into intermediate populations, and modified by means of crossover and mutation operators. Note that, at each iteration, each individual $C_i$ belonging to the current population codifies for an ordered set $\mathcal{L}_{out,i} = [C_i(1), \ldots, C_i(n)] = [l_{out,i}^{(min)}, \ldots, l_{out,i}^{(max)}]$, which represents a modified gray level distribution of $\mathcal{L}'_{in}$. In order to simplify the notation, in what follows we do not explicitly express that, *at each iteration*, each individual $C_i$ is (possibly) represented by a different circular array corresponding to $\mathcal{L}_{out}$.

For the selection of individuals, MedGA exploits a *tournament* strategy for three main reasons: (*i*) the selection pressure can be controlled by setting the tournament size $k$ (with $k \ll |P|$); (*ii*) the fitness evaluations are performed only on the $k$ individuals selected for the tournaments, and not on the whole population; (*iii*) this technique could be easily implemented on parallel architectures (Miller & Goldberg, 1995).

A *single point crossover* operator is applied with a given probability $p_c$ to the individuals selected by the tournament strategy and belonging to the first intermediate population $P'$. Namely, given two parent individuals $C_m, C_f \in P'$ (for some $m, f = 1, \ldots, |P|$), a crossover point is randomly selected from the circular arrays $[C_m(1), C_m(2), \ldots, C_m(n)]$ and $[C_f(1), C_f(2), \ldots, C_f(n)]$ encoding the individuals, and two offspring are generated by swapping 50% of the values between the two parents. The offspring are then inserted into a second intermediate population $P''$.

The *mutation* operator is applied with probability $p_m$ to each element $C_i(j) \in C_i = [l_{out,i}^{(min)}, \ldots, l_{out,i}^{(max)}]$ of each individual belonging to $P''$, where $l_{out,i}^{(min)}$ and $l_{out,i}^{(max)}$ are the minimum and maximum nonzero gray levels encoded by $C_i$ during the current iteration, respec-

tively. In particular, if the gray level intensity encoded in $C_i(j)$ is smaller than the optimal threshold $\theta_{opt,\,i}$ evaluated by IOTS at that iteration for the individual $C_i$, then an integer is randomly sampled from the uniform distribution in $[l_{out,i}^{(min)}, \ldots, \theta_{opt,i} - 1] \subset \mathbb{N}$ to update the value $C_i(j)$; otherwise, an integer is randomly sampled from the uniform distribution in $[\theta_{opt,i}, \ldots, l_{out,i}^{(max)}] \subset \mathbb{N}$ to update the value $C_i(j)$.

Finally, to prevent the quality of the best solution from decreasing during the optimization, MedGA also exploits an *elitism* strategy, so that the best individual from the current population is copied into the next population without undergoing the genetic operators.

Fig. 2 illustrates the overall procedure of MedGA, by presenting the initialization phase as well as the flow diagram of the proposed GA for image enhancement. The final best solution shows the achieved result on MRI data characterized by a bimodal histogram, emphasizing the two underlying distributions for the subsequent image thresholding phase, according to the optimal adaptive threshold $\theta_{opt}$, computed on the final best solution $C_{best}$, by using the simple IOTS algorithm (Ridler & Calvard, 1978; Trussell, 1979).

To evaluate the quality of the individuals throughout the optimization, the fitness function has been conceived to obtain a bimodal histogram in the gray levels intensities, therefore facilitating further automated image processing phases. The fitness function $\mathcal{F}(\cdot)$ used by MedGA fosters individuals $C_i$ characterized by a histogram with two well separated normal distributions, having an equal distance from the optimal threshold $\theta_{opt,\,i}$. To this purpose, at each iteration MedGA estimates, by using the efficient IOTS algorithm (Ridler & Calvard, 1978; Trussell, 1979), the mean values $\mu_{1,\,i}$ and $\mu_{2,\,i}$ of the two components $\mathcal{H}_{1,i}$ and $\mathcal{H}_{2,i}$ of the histogram $\mathcal{H}_i$, encoded by each individual $C_i$, according to the current optimal threshold $\theta_{opt,\,i}$. Afterwards, at each iteration the fitness function of every individual $C_i$ is calculated as follows:

$$
\begin{aligned}
\mathcal{F}(C_i) &= \tau_1 + \tau_2 + \tau_3, \quad \text{where:} \\
\tau_1 &= |2 \cdot \theta_{opt,i} - \mu_{1,i} - \mu_{2,i}|, \\
\tau_2 &= |\omega_{1,i} - 3\sigma_{1,i}|, \\
\tau_3 &= |\omega_{2,i} - 3\sigma_{2,i}|.
\end{aligned}
\tag{1}
$$

The terms $\omega_{1,i} = \frac{1}{2}(\theta_{opt,i} - \min_{j \in \{1,\ldots,n\}}\{C_i(j)\})$ and $\omega_{2,i} = \frac{1}{2}(\max_{j \in \{1,\ldots,n\}}\{C_i(j)\} - \theta_{opt,i})$ correspond to the half width of $\mathcal{H}_{1,i}$ and $\mathcal{H}_{2,i}$, respectively, while $\sigma_{1,\,i}$ and $\sigma_{2,\,i}$ are the standard deviations of $\mathcal{H}_{1,i}$ and $\mathcal{H}_{2,i}$, respectively. The three terms of the fitness function $\mathcal{F}(\cdot)$ cooperate together to achieve the desired image enhancement: $\tau_1$ aims at maintaining the mean values $\mu_{1,\,i}$ and $\mu_{2,\,i}$ equidistant from the yielded optimal threshold $\theta_{opt,\,i}$, while $\tau_2$ and $\tau_3$ are designed to force the sub-histograms $\mathcal{H}_{1,i}$ and $\mathcal{H}_{2,i}$ to approximate normal distributions.

We exploit the empirical property of normal distributions related to the coverage probability with respect the standard deviation. To be more precise, we consider the so-called 3-$\sigma$ rule, which states that approximately 99.73% of the values lie within $3\sigma$ according to: $Pr(\mu - 3\sigma \leq X \leq \mu + 3\sigma) \approx 0.9973$, where $\mu$, $\sigma$ and $X$ represent the mean, the standard deviation and an observation from a normally distributed random variable, respectively.

Examples of MR image enhancement results, achieved by MedGA on uterine fibroid, are shown in Fig. 3. MedGA enhances the input MR image by making uterine fibroid regions more uniform and with strong edges in terms of both visual human perception and automated image processing. The histogram in Fig. 3d proves that the output image is characterized by a more defined bimodal distribution compared to the initial image (Fig. 3b), which roughly tends to a trimodal gray level distribution.

It is worth noting that, in the case of further automated analysis, ROI pixel classification can be carried out by means of a basic threshold-based segmentation approach, since MR images enhanced with MedGA reveal a more precise separation between the two (possibly overlapping) sub-distributions in the histogram. Accordingly, MedGA allows for dealing with image histograms that do not meet the assumptions imposed by thresholding techniques, regarding bimodal histograms composed of two nearly Gaussian distributions with almost equal size and variance (Xue & Zhang, 2012). Indeed, MedGA enhances the image thresholding results on MRI data, as shown in Fig. 2, where the final best solution improves the underlying bimodal nature of the input histogram.

A sequential and a parallel version of MedGA have been implemented. The sequential version has been entirely developed using the Python programming language (version 2.7.12), while the parallel version is based on a Master-Slave paradigm employing `mpi4py`, which provides bindings of the Message Passing Interface (MPI) specifications for Python to leverage High-Performance Computing (HPC) resources (Dalcín, Paz, & Storti, 2005).

## 4. Materials and evaluation metrics

### 4.1. MRI dataset

Eighteen patients affected by symptomatic uterine fibroids, who underwent MRgFUS therapy, were taken into account. The total number of the examined fibroids was 29 represented on 163 CE MR slices, since some patients presented a pathological scenario with multiple fibroids. The analyzed images were acquired using a Signa HDxt MRI scanner (General Electric Medical Systems, Milwaukee, WI, USA) at two different institutions. These MRI data were acquired after the MRgFUS treatment, executed with the Ex-Ablate 2100 (Insightec Ltd., Carmel, Israel) HIFU equipment. The considered MRI series were scanned using the T1w "Fast Spoiled Gradient Echo + Fat Suppression + Contrast mean" (FSPGR+FS+C) protocol. This MRI protocol is usually employed for Non-Perfused Volume (NPV) assessment (Gorny et al., 2011), since ablated fibroids appear as hypo-intense areas due to low perfusion of the contrast medium. Sagittal MRI sections were processed, in compliance with the current clinical practice for therapy response assessment (Militello, Rundo, & Gilardi, 2014). MRI acquisition parameters were: Repetition Time (TR): $150 - 260$ ms; Echo Time (TE): $1.392 - 1.544$ ms; pixel depth: 16-bit; matrix size: $512 \times 512$ pixels; slice thickness: 5.0 mm; slice spacing: 6.0 mm; pixel spacing: $0.6641 - 0.7031$ mm.

As explained in Section 3, before applying MedGA image enhancement, the uterus region (i.e., ROI bounding region) must be delineated. This task can be accomplished manually by the user or automatically by means of computational methods to reduce operator-dependency, as previously proposed in Militello et al. (2015b). Afterwards, the pixels with values lower than the optimal threshold $\theta_{opt}$, computed by means of the efficient IOTS method (Ridler & Calvard, 1978; Trussell, 1979), are segmented in the binarized MR image. In this clinical scenario, segmentation approaches must deal with NPV inhomogeneities, due to sonication spots during the MRgFUS treatment.

### 4.2. Image enhancement evaluation metrics

In this section, we recall the definition of the metrics typically used to evaluate image enhancement approaches, which will be exploited to assess the performance of MedGA. These metrics are essential to quantitatively evaluate the effects of image enhancement techniques, since measuring the "quality" of an image might be strongly subjective. In particular, we benefit here from the metrics considered in Hashemi et al. (2010) to assess the capability of
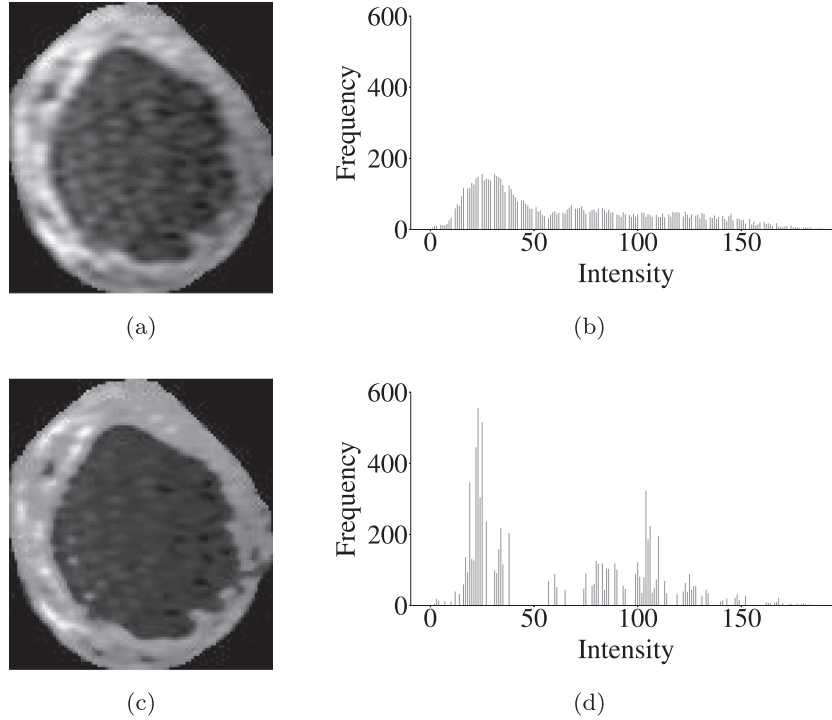
**Fig. 3.** Enhanced image obtained by MedGA on uterine fibroids of patients who had undergone MRgFUS therapy: (a) input MR image normalized by using linear contrast stretching on the initial full range of the masked MR image; (c) output image after the application of MedGA. Plots (b) and (d) report the histograms of gray level intensities corresponding to the MR images in (a) and (c), respectively.

image enhancement approaches in improving contrast, details and human visual perception.

Let $I_{orig}$ and $I_{enh}$ be the original input image and the enhanced image, respectively, consisting in $M$ rows and $N$ columns. Considering that the range of gray levels of the output image $\mathcal{L}_{out} = [l_{out}^{(min)}, \ldots, l_{out}^{(max)}]$ could be different from the original range $\mathcal{L}_{in} = [l_{in}^{(min)}, \ldots, l_{in}^{(max)}]$, as a first step before computing the metrics we remap the output pixel intensities (i.e., the gray levels) into the original range, as follows:

$$\tilde{I}_{enh}(a, b) = \frac{(I_{enh}(a, b) - l_{out}^{(min)}) \cdot (l_{in}^{(max)} - l_{in}^{(min)})}{(l_{out}^{(max)} - l_{out}^{(min)})} + l_{in}^{(min)}, \qquad (2)$$

where $a = 1, \ldots, M$ and $b = 1, \ldots, N$. Note that we actually consider the extended range $\mathcal{L}'_{in}$ for $I_{orig}$, as explained in Section 3.

The Peak Signal-to-Noise Ratio (*PSNR*) denotes the ratio between the maximum possible intensity value of a signal and the distortion between the input and output images:

$$\begin{aligned} PSNR &= 10 \cdot \log_{10}\left(\frac{(l_{in}^{(max)})^2}{MSE}\right) \\ &= 20 \cdot \log_{10}\left(\frac{l_{in}^{(max)}}{\sqrt{MSE}}\right), \end{aligned} \qquad (3)$$

where $MSE = \frac{1}{M \times N} \sum_{a=1}^{M} \sum_{b=1}^{N} ||I_{orig}(a, b) - \tilde{I}_{enh}(a, b)||^2$ is the Mean Squared Error, which allows us to compare the pixel values of $I_{orig}$ to those of $\tilde{I}_{enh}$.

Furthermore, the *PSNR* is usually expressed in terms of the logarithmic Decibel scale. With regard to our application, we employ only a limited portion of the full dynamic range of the 16-bit images (see Section 3); we thus use as the largest possible value the maximum intensity value present in the original image (i.e., $l_{in}^{(max)} = \max\{\mathcal{L}_{in}\} = \max\{\mathcal{L}'_{in}\}$) instead of the maximum representable value in a 16-bit image (i.e., $2^{16} - 1 = 65,535$).

Munteanu and Rosa (2004) stated that good contrast and enhanced images are characterized by high numbers of *edgels* (i.e., pixels belonging to an edge), and that an enhanced image should

have a higher intensity of the edges, compared to its non-enhanced counterpart (Saitoh, 1999). Therefore, a good enhancement technique should yield satisfactory results in the case of standard vision processing tasks, such as segmentation or edge detection (Starck, Murtagh, Candes, & Donoho, 2003). Here, to evaluate image enhancement of MRI data, we employ the method proposed by Canny (1986), which is a highly reliable and mathematically well-defined edge detector. This approach deals with weak edges and accurately determines edgels, by applying a double threshold (to identify potential edges) and a hysteresis-based edge tracking. Let $\mathcal{M}_{Canny}$ be the edge map yielded by the Canny's edge detector, which is a binary image wherein only edgels are set to 1. The number of detected edges (#DE) in $\mathcal{M}_{Canny}$ is computed as:

$$\#DE = \sum_{a=1}^{M} \sum_{b=1}^{N} \mathcal{M}_{Canny}(a, b). \qquad (4)$$

An additional metrics, called Absolute Mean Brightness Error (*AMBE*) (Arriaga-Garcia, Sanchez-Yanez, & Garcia-Hernandez, 2014; Chen & Ramli, 2003), can be employed to measure the brightness preservation of the enhanced image:

$$AMBE = \frac{|\mathbb{E}[I_{orig}] - \mathbb{E}[\tilde{I}_{enh}]|}{L}, \qquad (5)$$

where $\mathbb{E}[\cdot]$ denotes the expected (mean) value of a gray level distribution. *AMBE* is normalized in [0,1], divided by $L = l_{in}^{(max)} - l_{in}^{(min)}$, which is the dynamic range of the input gray-scale (in our case, $\mathcal{L}'_{in}$). Note that low values of *AMBE* denote that the mean brightness of the original image is preserved.

Finally, we consider an alternative quality metrics called Structural Similarity Index (*SSIM*) (Wang, Bovik, Sheikh, & Simoncelli, 2004), used to assess the image degradation perceived as variations in structural information (Bhandari, Kumar, Chaudhary, & Singh, 2016). The structural information defines the attributes that represent the structure of objects in the image, independently of the average luminance and contrast. In particular, local luminance

and contrast are taken into account since overall values of luminance and contrast can remarkably vary across the whole image. *SSIM* is based on the degradation of structural information—assuming that human visual perception is highly adapted for extracting structural information from a scene—and compares local patterns of pixel intensities. As a matter of fact, natural image signals are highly structured, since pixels are strongly dependent on each other, especially those close by. These dependencies convey important information about the structure of the objects in the viewing field. Let **X** and **Y** be the $I_{orig}$ and $I_{enh}$ image signals, respectively; *SSIM* combines three relatively independent terms:

- the luminance comparison $l(\mathbf{X}, \mathbf{Y}) = \frac{2\mu_{\mathbf{X}}\mu_{\mathbf{Y}} + \kappa_1}{\mu_{\mathbf{X}}^2 + \mu_{\mathbf{Y}}^2 + \kappa_1}$;
- the contrast comparison $c(\mathbf{X}, \mathbf{Y}) = \frac{2\sigma_{\mathbf{X}}\sigma_{\mathbf{Y}} + \kappa_2}{\sigma_{\mathbf{X}}^2 + \sigma_{\mathbf{Y}}^2 + \kappa_2}$;
- the structural comparison $s(\mathbf{X}, \mathbf{Y}) = \frac{\sigma_{\mathbf{XY}} + \kappa_3}{\sigma_{\mathbf{X}}\sigma_{\mathbf{Y}} + \kappa_3}$;

where $\mu_{\mathbf{X}}$, $\mu_{\mathbf{Y}}$, $\sigma_{\mathbf{X}}$, $\sigma_{\mathbf{Y}}$, and $\sigma_{\mathbf{XY}}$ are the local means, standard deviations, and cross-covariance for the images **X** and **Y**, while $\kappa_1, \kappa_2, \kappa_3 \in \mathbb{R}^+$ are regularization constants for luminance, contrast, and structural terms, respectively, exploited to avoid instability in the case of image regions characterized by local mean or standard deviation close to zero. Typically, small non-zero values are employed for these constants; according to Wang et al. (2004), an appropriate setting is $\kappa_1 = (0.01 \cdot L)^2$, $\kappa_2 = (0.03 \cdot L)^2$, $\kappa_3 = \kappa_2/2$, where $L$ is the dynamic range of the pixel values in $I_{orig}$ (represented in $\mathcal{L}'_{in}$). *SSIM* is then computed by combining the components described above:

$$SSIM = l(\mathbf{X}, \mathbf{Y})^{\alpha} \cdot c(\mathbf{X}, \mathbf{Y})^{\beta} \cdot s(\mathbf{X}, \mathbf{Y})^{\gamma}, \qquad (6)$$

where $\alpha, \beta, \gamma > 0$ are weighting exponents. As reported in Wang et al. (2004), if $\alpha = \beta = \gamma = 1$ and $\kappa_3 = \kappa_2/2$, the *SSIM* becomes:

$$SSIM = \frac{(2\mu_{\mathbf{X}}\mu_{\mathbf{Y}} + \kappa_1)(2\sigma_{\mathbf{XY}} + \kappa_2)}{\left(\mu_{\mathbf{X}}^2 + \mu_{\mathbf{Y}}^2 + \kappa_1\right)\left(\sigma_{\mathbf{X}}^2 + \sigma_{\mathbf{Y}}^2 + \kappa_2\right)}. \qquad (7)$$

*SSIM* generalizes the Universal Quality Index (*UQI*), defined in Wang and Bovik (2002), which is obtained by setting $\kappa_1 = \kappa_2 = 0$, and yields unstable results when either $\left(\mu_{\mathbf{X}}^2 + \mu_{\mathbf{Y}}^2\right)$ or $\left(\sigma_{\mathbf{X}}^2 + \sigma_{\mathbf{Y}}^2\right)$ tends to zero. Notice that the higher the *SSIM* value, the higher the structural similarity, implying that the enhanced image $I_{enh}$ and the original image $I_{orig}$ are quantitatively similar.

## 5. Results

This section presents the experimental results achieved by our image enhancement method. We first analyze the performances of MedGA by varying the parameter settings of the GA at the basis of our methodology; we then compared it against the most common and popular image enhancement techniques in the image processing field (see Gonzalez and Woods (2002) for additional details).

### 5.1. MedGA settings analysis and calibration

To analyze the performances of MedGA and identify the best settings for the image enhancement problem, we considered a calibration set consisting of 80 medical images randomly selected from the available MRI data (described in Section 4.1), and we varied the settings of MedGA used throughout the optimization process, that is: (*i*) the size of the population $|P| \in \{50, 100, 150, 200\}$; (*ii*) the crossover probability $p_c \in \{0.8, 0.85, 0.9, 0.95, 1.0\}$; (*iii*) the mutation probability $p_m \in \{0.01, 0.05, 0.1, 0.2\}$; (*iv*) the size of the tournament selection strategy $k \in \{5, 10, 15, 20\}$. In all tests, MedGA was run for $T = 100$ iterations. Each MedGA execution was performed by varying one setting at a time, for a total of 320 different settings tested and a total number of $320 \times 80 = 25600$ MedGA executions.
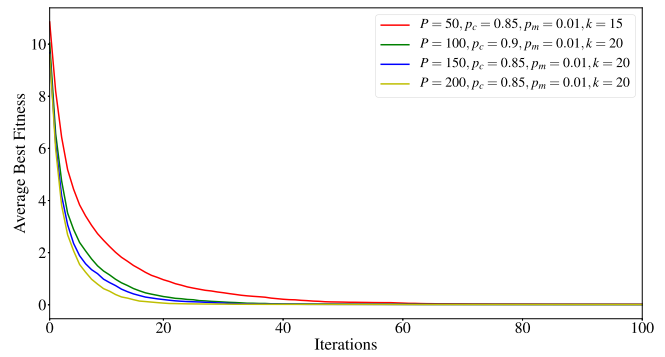


**Fig. 4.** Comparison of the ABF achieved by MedGA with the best parameterizations found for each value of |P| tested here. The average was computed over the results of the optimization of 80 MR images.

The results of these tests (data not shown) highlighted that, for each value of |P|, the best settings in terms of fitness values achieved are:

1. $|P| = 50$, $p_c = 0.85$, $p_m = 0.01$, $k = 15$;
2. $|P| = 100$, $p_c = 0.9$, $p_m = 0.01$, $k = 20$;
3. $|P| = 150$, $p_c = 0.85$, $p_m = 0.01$, $k = 20$;
4. $|P| = 200$, $p_c = 0.85$, $p_m = 0.01$, $k = 20$.

Fig. 4 reports the comparison of the performances achieved by MedGA with these settings, where the Average Best Fitness (ABF) was computed by taking into account, at each iteration of MedGA, the fitness value of the best individuals over the 80 optimization processes. It is clear from the plot that, despite the final ABF values are comparable in all settings, the convergence speed increases with the size of the population, as well as the running time required by MedGA; therefore, to choose the best settings, we analyzed the computational performances concerning the 4 tests listed above.

Considering that an MRI series related to a single patient contains on average 10 slices with ROI fibroids, we tested the clinical feasibility of MedGA by calculating the total execution time for enhancing 10 randomly chosen MR images. For what concerns the tests 1–4 described above, the executions lasted on average 672.12 s, 1290.15 s, 1987.8 s, and 2669.74 s, respectively, for the optimization of the same batch of 10 images running a single core of the Intel Xeon E5-2440 CPU with 2.40 GHz clock frequency. On the other hand, by exploiting the 6 cores of the same CPU to execute the parallel version of MedGA, we achieved up to $3.6 \times$ speed-up with respect to the sequential version. The results achieved using the parallel version of MedGA confirm the importance of HPC solutions in the field of real healthcare environment to obtain clinically feasible outcomes, that is, enhancing MR images in reasonable time for medical imaging practice.

By considering both the performance of MedGA in terms of ABF and the running time required to process 80 images, we selected the parameter settings $|P| = 100$, $p_c = 0.9$, $p_m = 0.01$, $k = 20$ as the best trade-off characterized by a good convergence speed and an adequate running time (for this specific application), and we exploited this configuration for all tests reported and discussed in the following section.

### 5.2. Comparison with state-of-the-art methods

The performances of MedGA were compared against the following image enhancement techniques:

- Histogram Equalization (HE) (Hall, 1974; Paranjape, 2009), which adjusts pixel intensities for contrast enhancement according to the normalized histogram of the original image $I_{orig}$.
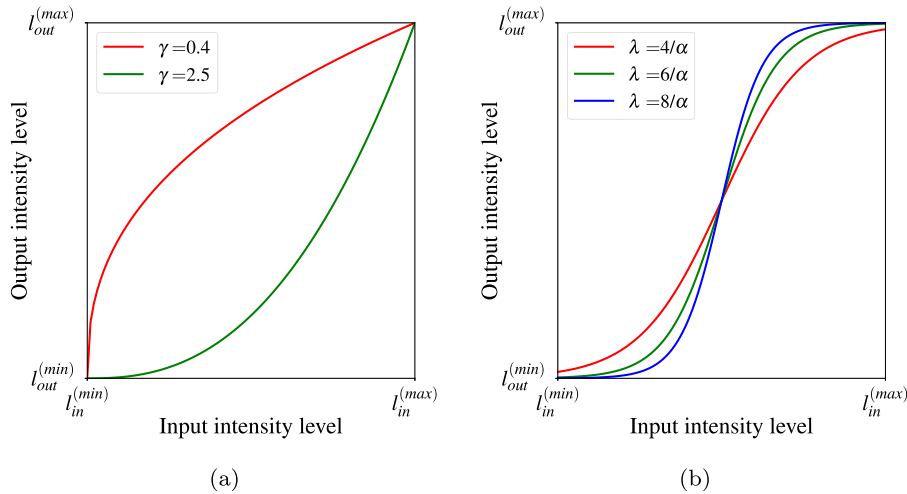
**Fig. 5.** Plots of the implemented global non-linear intensity transformations for image enhancement: (a) Gamma Transformation; (b) Sigmoid intensity Transformation. We report on the *x*-axis the input intensity range $[l_{in}^{(min)}, \ldots, l_{in}^{(max)}]$, and on the *y*-axis the output intensity range $[l_{out}^{(min)}, \ldots, l_{out}^{(max)}]$.

With HE, gray levels are more uniformly distributed on the histogram, by spreading the most frequent intensity values;

- Bi-Histogram Equalization (Bi-HE) (Kim, 1997)—a modification of the traditional HE—that addresses issues concerning mean brightness preservation;
- Gamma Transformation (GT), which is a non-linear operation using the power-law relationship $s(r) = cr^{\gamma}$, where $r$ and $s$ are the input and the output gray-scale values, respectively, and $c$ is a multiplication constant ($c = 1$ in the following tests). The parameter $\gamma$ is set to values greater than 1 (i.e., decoding gamma) to obtain a gamma expansion, or to values smaller than 1 (i.e., encoding gamma) to realize a gamma compression (see Fig. 5a). In our tests we considered the values $\gamma = 0.4$ and $\gamma = 2.5$, as higher (lower) values of $\gamma$ tend to logarithmic (anti-logarithmic) functions, resulting in an excessively bright (dark) output image, unsuitable for practical medical applications (Gandhamal et al., 2017);
- Sigmoid intensity Transformation (ST) function (Fig. 5b), also called S-shaped curve, which is a global non-linear mapping defined as follows:

$$s(r) = \frac{l_{in}^{(max)}}{1 + \exp\left(-\lambda(r - \alpha)\right)}, \tag{8}$$

where $l_{in}^{(max)} = \max\{\mathcal{L}_{in}\} = \max\{\mathcal{L}'_{in}\}$ is the asymptotic maximum value of the function, $\alpha = \frac{1}{2}\left(l_{in}^{(max)} - l_{in}^{(min)}\right)$ is the midpoint value, and $\lambda$ defines the function steepness. This transformation stretches the intensity around the level $\alpha$, by making the hypo-intense histogram part darker and the hyper-intense histogram part brighter. Thus, the difference between the minimum and maximum gray values and the gradient magnitude of the image are increased, obtaining strong edges (Gandhamal et al., 2017). In our tests, we used sigmoid functions that allow for considering the entire input dynamic range, by varying the curve slope with the values $\lambda \in \left\{ \frac{4}{\alpha}, \frac{6}{\alpha}, \frac{8}{\alpha} \right\}$.

In order to achieve a thorough comparison between MedGA and the enhancement techniques listed above, we exploited the entire set of MRI data consisting in 163 medical images of uterine fibroids (including both calibration and unseen data). For each technique, we computed the metrics *PSNR*, #DE, *AMBE, SSIM* defined in Section 4.2. The resulting values are given in Fig. 6 (boxplots) and in Table 1 (median, mean and standard deviation). Overall, these results highlight that MedGA significantly outperforms the conventional image enhancement approaches in terms of signal quality

and perceived structural information in the images, while preserving the input mean brightness. As a matter of fact, MedGA achieves the highest *PSNR* and *SSIM* median and mean values (see Fig. 6 and Table 1). Concerning the other enhancement techniques, we observe that Bi-HE achieves better performances with respect to HE, while increasing the values of $\gamma$ and $\lambda$ corresponds to a degradation of the performances of GT and ST, respectively.

For what concerns the #DE metrics, HE over-enhances the processed MR images, as denoted by the highest median and mean values achieved, while Bi-HE allows for the preservation of the mean brightness, as also indicated by the lowest mean value of *AMBE*. On the contrary, GT achieved the worst performance in terms of *AMBE* metrics. This poor result is due to the intrinsic nature of GT that transforms the input gray-scale range into a darker ($\gamma > 1$) or brighter ($\gamma < 1$) one, by increasing the number of hyper-intense and hypo-intense pixels, respectively. By doing so, GT does not preserve the input mean brightness, thus obtaining the highest values of *AMBE*. All the other methods are characterized by comparable #DE values, while the *PSNR* is characterized by very high mean values in the case of GT with respect to the other techniques. On the one hand, considering the *SSIM* metrics, GT with $\gamma = 0.4$ remarkably yields better results compared to GT with $\gamma = 2.5$, especially in the case of the *SSIM*; on the other hand, all metrics related to the tested ST functions show that their performances decrease as the value of $\lambda$ increases. This phenomenon is related to the rapid variation characterizing the highest values of $\lambda$, which do not allow for taking into consideration the existing dependency among the pixels, especially those in the neighborhood.

Finally, we show in Fig. 7 two examples of MR images enhanced by using all the methods considered in this work. As it can be observed, MedGA strengthens the ROI edges by enhancing details and features useful for image binarization; this result confirms, from a qualitative perspective, the quantitative results presented above.

From an overall view of the metrics, we can claim that the approaches obtaining the highest values of the #DE measure (i.e., HE and GT with $\gamma = 2.5$) could imply an over-enhancement of the output image, according to the other image quality metrics. This finding is also confirmed by means of a visual inspection of Fig. 7, where the images enhanced using HE and GT with $\gamma = 2.5$ present an inadequate appearance for image observation and interpretation. To conclude, MedGA achieves outstanding results in performance evaluation with respect to classic image enhancement techniques.
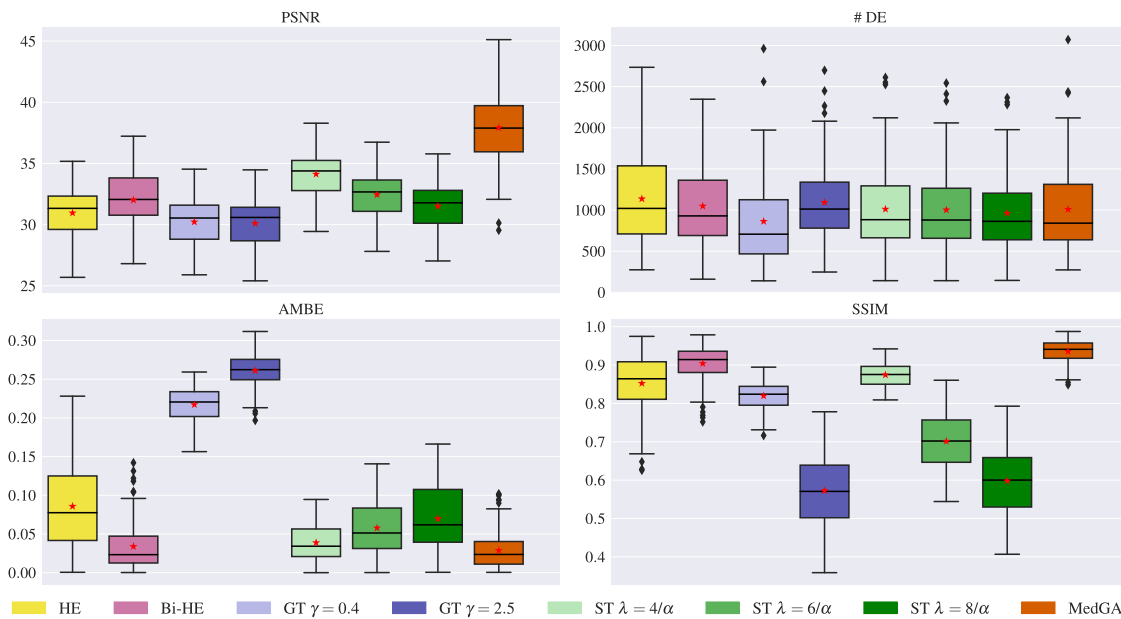
**Fig. 6.** Boxplots of the image enhancement evaluation metrics considered in this work, obtained on an MRI dataset composed of 18 patients with uterine fibroids who had undergone MRgFUS treatment (total number of MR slices: 163). The lower and the upper bounds of each box represent the first and third quartiles of the statistical distribution, respectively, corresponding to the interquartile range. The median and the mean values are represented by a black solid line and a red star, respectively. Whiskers value is 1.5 in all cases and outliers are displayed as black diamonds. (For interpretation of the references to color in this figure legend, the reader is referred to the web version of this article.)

**Table 1**

Median, mean and standard deviation of image enhancement evaluation metrics achieved by HE, Bi-HE, GT (with $\gamma \in \{0.4, 2.5\}$), ST (with $\lambda \in \{4/\alpha, 6/\alpha, 8/\alpha\}$) and MedGA, considering the uterine fibroid MRI dataset consisting in a total of 163 medical images.

| | PSNR | | | #DE | | | AMBE | | | SSIM | | |
|---|---|---|---|---|---|---|---|---|---|---|---|---|
| | *Median* | *Mean* | *Std. Dev.* | *Median* | *Mean* | *Std. Dev.* | *Median* | *Mean* | *Std. Dev.* | *Median* | *Mean* | *Std. Dev.* |
| HE | 31.331 | 30.957 | 2.068 | 1020 | 1136.865 | 561.791 | 0.077 | 0.086 | 0.053 | 0.864 | 0.852 | 0.072 |
| Bi-HE | 32.059 | 32.014 | 2.232 | 929 | 1048.301 | 472.550 | 0.023 | 0.034 | 0.029 | 0.914 | 0.904 | 0.046 |
| GT $\gamma = 0.4$ | 30.540 | 30.223 | 1.994 | 707 | 862.871 | 510.196 | 0.221 | 0.217 | 0.022 | 0.824 | 0.820 | 0.033 |
| GT $\gamma = 2.5$ | 30.588 | 30.106 | 2.063 | 1012 | 1092.847 | 444.502 | 0.262 | 0.261 | 0.021 | 0.571 | 0.573 | 0.094 |
| ST $\lambda = 4/\alpha$ | 34.389 | 34.127 | 1.880 | 883 | 1011.061 | 468.799 | 0.034 | 0.039 | 0.024 | 0.875 | 0.874 | 0.031 |
| ST $\lambda = 6/\alpha$ | 32.673 | 32.449 | 1.950 | 879 | 1002.196 | 443.344 | 0.051 | 0.058 | 0.035 | 0.702 | 0.701 | 0.074 |
| ST $\lambda = 8/\alpha$ | 31.782 | 31.513 | 1.983 | 863 | 962.141 | 411.109 | 0.062 | 0.070 | 0.042 | 0.600 | 0.598 | 0.089 |
| MedGA | 37.891 | 37.914 | 2.821 | 841 | 1008.773 | 499.906 | 0.024 | 0.029 | 0.023 | 0.941 | 0.936 | 0.029 |
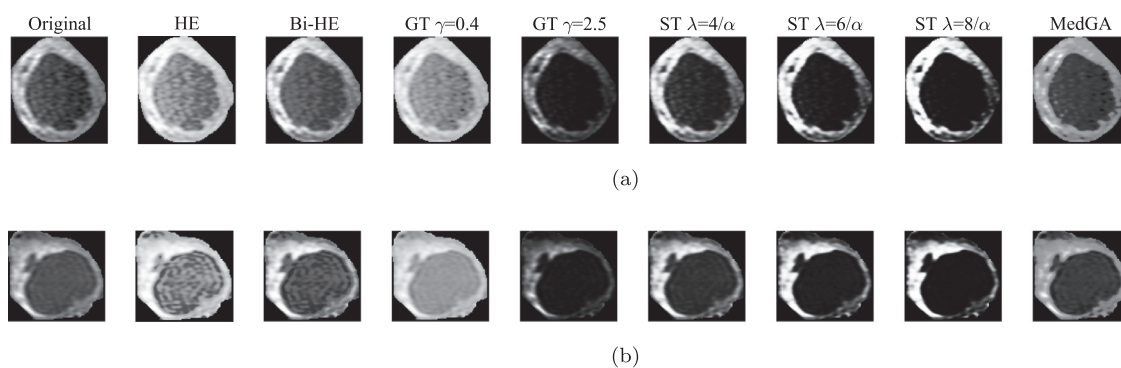


**Fig. 7.** Examples of enhancement achieved on medical images of uterine fibroids by HE, Bi-HE, GT (with $\gamma \in \{0.4, 2.5\}$), ST (with $\lambda \in \{4/\alpha, 6/\alpha, 8/\alpha\}$) and MedGA, compared with the original input MR image.

## 6. Discussion

The main purpose of state-of-the-art methods for image enhancement is the improvement of the contrast level of the whole image, to obtain a "visually pleasant" result. On the contrary, MedGA is the first enhancement method that explicitly addresses the challenging issues related to the improvement of medical images that are characterized by a nearly bimodal gray level histogram distribution. The solution provided by our intelligent image enhancement system can be beneficial to visually assist physicians in interactive decision-making tasks, as well as to improve the final outcome of downstream automated processing pipelines for useful measurements in the clinical practice (Rueckert et al., 2016).

MedGA also deals with the practical problems regarding the interpretability of the results yielded by advanced Machine Learning and Computational Intelligence methods in medicine

(Cabitza et al., 2017). Indeed, the final best solution found by MedGA (i.e., the output gray level histogram) and the corresponding enhanced image are understandable by physicians. In addition, the efficient encoding of the individuals—taking inspiration by Hashemi et al. (2010)—coupled with effective HPC solutions, allows for a clinically feasible computational framework. We designed a specific fitness function to emphasize the two Gaussian distributions composing a bimodal histogram, while the existing approaches based on evolutionary computation or Swarm Intelligence techniques were conceived for a different purpose, i.e., improving the perceived visual information in terms of image contrast. Thanks to this *ad hoc* fitness function—differently to the GP-based image enhancement method in Poli and Cagnoni (1997), where no fitness function is defined because the user interactively selects the best solution—and the robustness achieved by means of the calibration step for GA's parameter setting, MedGA does not require any user interaction step. Moreover, MedGA differs from GP-based approaches, in which the final generated solution could have large size (Castelli et al., 2014), so heavily affecting the readability and interpretability of the provided solutions. The main impact of this contribution consists in showing how an effective method based on evolutionary computation can outperform the existing methods in medical image enhancement.

In this work, we tested and validated our approach on MR images regarding MRgFUS therapy for uterine fibroids. More generally, the application of MedGA can be extended also to real-world problems involving the analysis of images characterized by an underlying bimodal histogram, as in the case of bright-field and fluorescence microscopy imaging (Meijering, 2012).

Considering the achieved results in terms of #DE (see Table 1), MedGA's performance could be further improved—in terms of contrast—by integrating a novel component in the fitness function, which explicitly relies on the number of detected edges. Since this additional component would have a different purpose and a different magnitude, a multi-objective optimization method should be taken into account. In particular, MedGA could be extended by means of an effective evolutionary computation approach, such as NSGA-III (Deb & Jain, 2014), to simultaneously optimize both conflicting objectives, which consist in maximizing the number of edges while minimizing the distance between the optimal threshold and the two normal distributions.

## 7. Conclusion and future work

A novel image enhancement method based on GAs, specifically tailored for medical images characterized by a bimodal histogram, was proposed in this paper. This computational framework, named MedGA, exploits a fitness function that better reveals the two underlying sub-distributions of the gray level intensities, consequently allowing for an improvement in the results achieved by threshold-based algorithms. Unlike the traditional image enhancement techniques that generally improve the contrast level of the whole image, MedGA focuses on MR image sub-regions characterized by a roughly bimodal histogram, making it valuable in clinical contexts involving CE MRI analysis.

We tested and validated our approach on MR images representing uterine fibroids of patients who underwent MRgFUS therapy. MedGA was compared against the most common image enhancement techniques, overall achieving the best performances with respect to both signal and perceived image quality, while preserving, unlike classic HE techniques, the input mean brightness. This novel medical image enhancement technique was therefore shown to be a promising solution, suitable for medical expert systems.

We remark that, although MedGA exploits the same encoding of individuals defined in Hashemi et al. (2010) and Draa and Bouaziz (2014) we did not compare it to other approaches based on evolutionary computation or Swarm Intelligence techniques (see also (Chen et al., 2018)), since they were conceived for a different purpose, that is, improving the perceived visual information of the whole image. As a matter of fact, these approaches explicitly include in the fitness function both the number of edge pixels and the intensity of such pixels, thus achieving high #DE values that would consistently lead to over-enhanced images.

As a future extension of this work, in the case of large size images (e.g., $1000 \times 1000$ pixels) we plan to use Graphics Processing Units, which represent an enabling technology for real-time radiology applications (Eklund, Dufort, Forsberg, & LaConte, 2013), since the running time of histograms computation can be considerably reduced by using a parallel implementation (Scheuermann & Hensley, 2007).

In addition, we plan to integrate MedGA as a pre-processing step within an automatic pipeline defined in the context of MR image classification for efficient computer-assisted segmentation using thresholding techniques, such as (Otsu, 1975; Ridler & Calvard, 1978; Trussell, 1979). Indeed, MR image segmentation is a compelling task in radiology practice, for instance in brain tumor detection and delineation (Sompong & Wongthanavasu, 2017). Especially, we plan to apply MedGA to metastatic cancer segmentation in neuro-radiosurgery therapy (Leksell, 1949), wherein the enhancement region must be accurately segmented (Militello et al., 2015a; Rundo et al., 2017). In order to make the resulting expert system fully automatic, the segmentation of the ROI bounding region could be performed by robust computational methods that can ensure results repeatability during patients follow-up. In the case of a significant data availability, this step may be performed by means of approaches based on Deep Neural Networks (Rajchl et al., 2017). In these clinical scenarios, MedGA can be suitably integrated into expert systems tailored for MRgFUS treatment evaluation (Rundo et al., 2019), and brain tumor segmentation in neuro-radiosurgery (Meier et al., 2016).

## CRediT authorship contribution statement

**Leonardo Rundo:** Conceptualization, Methodology, Software, Validation, Formal analysis, Investigation, Resources, Data curation, Writing - original draft, Writing - review & editing, Visualization. **Andrea Tangherloni:** Conceptualization, Methodology, Software, Validation, Formal analysis, Investigation, Data curation, Writing - original draft, Writing - review & editing, Visualization. **Marco S. Nobile:** Methodology, Validation, Formal analysis, Writing - review & editing, Supervision. **Carmelo Militello:** Methodology, Validation, Formal analysis, Resources, Writing - review & editing, Supervision. **Daniela Besozzi:** Validation, Formal analysis, Writing - review & editing, Supervision, Project administration. **Giancarlo Mauri:** Resources, Writing - review & editing, Supervision, Funding acquisition. **Paolo Cazzaniga:** Methodology, Validation, Formal analysis, Writing - review & editing, Supervision, Project administration.

## Acknowledgment

## References

de Araujo, A. F., Constantinou, C. E., & Tavares, J. M. R. S. (2014). New artificial life model for image enhancement. *Expert Systems with Applications, 41*(13), 5892–5906. doi:10.1016/j.eswa.2014.03.029.

Arriaga-Garcia, E. F., Sanchez-Yanez, R. E., & Garcia-Hernandez, M. G. (2014). Image enhancement using bi-histogram equalization with adaptive sigmoid functions. In *Proc. IEEE international conference on electronics, communications and computers (CONIELECOMP)* (pp. 28–34). IEEE. doi:10.1109/CONIELECOMP.2014.6808563.

Bellon, E. M., Haacke, E. M., Coleman, P. E., Sacco, D. C., Steiger, D. A., & Gangarosa, R. E. (1986). MR artifacts: Areview. *American Journal of Roentgenology, 147*(6), 1271–1281. doi:10.2214/ajr.147.6.1271.

Bhandari, A. K., Kumar, A., Chaudhary, S., & Singh, G. (2016). A novel color image multilevel thresholding based segmentation using nature inspired optimization algorithms. *Expert Systems with Applications, 63*, 112–133. doi:10.1016/j.eswa.2016.06.044.

Bianco, S., Ciocca, G., & Schettini, R. (2017). Combination of video change detection algorithms by genetic programming. *IEEE Transactions on Evolutionary Computation, 21*(6), 914–928. doi:10.1109/TEVC.2017.2694160.

Brown, R. W., Cheng, Y. C. N., Haacke, E. M., Thompson, M. R., & Venkatesan, R. (2014). *Magnetic resonance imaging: Physical principles and sequence design*. John Wiley & Sons. doi:10.1002/9781118633953.

Cabitza, F., Rasoini, R., & Gensini, G. F. (2017). Unintended consequences of machine learning in medicine. *JAMA, 318*(6), 517–518. doi:10.1001/jama.2017.7797.

Canny, J. (1986). A computational approach to edge detection. *IEEE Transactions on Pattern Analysis and Machine Intelligence, PAMI-8*(6), 679–698. doi:10.1109/TPAMI.1986.4767851.

Carbonaro, A., & Zingaretti, P. (1999). A comprehensive approach to image-contrast enhancement. In *Proceedings of the international conference on image analysis and processing (ICIAP)* (pp. 241–246). IEEE. doi:10.1109/ICIAP.1999.797602.

Castelli, M., Vanneschi, L., & Silva, S. (2014). Prediction of the unified Parkinson's disease rating scale assessment using a genetic programming system with geometric semantic genetic operators. *Expert Systems with Applications, 41*(10), 4608–4616. doi:10.1016/j.eswa.2014.01.018.

Castelvecchi, D. (2016). Can we open the black box of AI? *National News, 538*(7623), 20. doi:10.1038/538020a.

Chen, C. M., Chen, C. C., Wu, M. C., Horng, G., Wu, H. C., Hsueh, S. H., & Ho, H. Y. (2015). Automatic contrast enhancement of brain MR images using hierarchical correlation histogram analysis. *Journal of Medical and Biological Engineering, 35*(6), 724–734. doi:10.1007/s40846-015-0096-6.

Chen, J., Yu, W., Tian, J., Chen, L., & Zhou, Z. (2018). Image contrast enhancement using an artificial bee colony algorithm. *Swarm and Evolutionary Computation, 38*, 287–294. doi:10.1016/j.swevo.2017.09.002.

Chen, S. D., & Ramli, A. R. (2003). Minimum mean brightness error bi-histogram equalization in contrast enhancement. *IEEE Transactions on Consumer Electronics, 49*(4), 1310–1319. doi:10.1109/TCE.2003.1261234.

Dalcín, L., Paz, R., & Storti, M. (2005). MPI For python. *Journal of Parallel and Distributed Computing, 65*(9), 1108–1115. doi:10.1016/j.jpdc.2005.03.010.

Deb, K., & Jain, H. (2014). An evolutionary many-objective optimization algorithm using reference-point-based nondominated sorting approach, part i: Solving problems with box constraints. *IEEE Transactions on Evolutionary Computation, 18*(4), 577–601. doi:10.1109/TEVC.2013.2281535.

Draa, A., & Bouaziz, A. (2014). An artificial bee colony algorithm for image contrast enhancement. *Swarm and Evolutionary Computation, 16*, 69–84. doi:10.1016/j.swevo.2014.01.003.

Eklund, A., Dufort, P., Forsberg, D., & LaConte, S. M. (2013). Medical image processing on the GPU – Past, present and future. *Medical Image Analysis, 17*(8), 1073–1094. doi:10.1016/j.media.2013.05.008.

Evans, P. M. (2008). Anatomical imaging for radiotherapy. *Physics in Medicine and Biology, 53*(12), R151. doi:10.1088/0031-9155/53/12/R01.

Gan, H. S., Swee, T. T., Abdul Karim, A. H., Sayuti, K. A., Abdul Kadir, M. R., Tham, W. K., et al. (2014). Medical image visual appearance improvement using bihistogram bezier curve contrast enhancement: Data from the osteoarthritis initiative. *The Scientific World Journal, 2014*(294104), 1–13. doi:10.1155/2014/294104.

Gandhamal, A., Talbar, S., Gajre, S., Hani, A. F. M., & Kumar, D. (2017). Local gray level s-curve transformation–a generalized contrast enhancement technique for medical images. *Computers in Biology and Medicine, 83*, 120–133. doi:10.1016/j.compbiomed.2017.03.001.

Gonzalez, R. C., & Woods, R. E. (2002). *Digital image processing* (3rd). Upper Saddle River, NJ, USA: Prentice Hall Press.

Gorny, K. R., Woodrum, D. A., Brown, D. L., Henrichsen, T. L., Weaver, A. L., Amrami, K. K., et al. (2011). Magnetic resonance–guided focused ultrasound of uterine leiomyomas: Review of a 12-month outcome of 130 clinical patients. *Journal of Vascular and Interventional Radiology, 22*(6), 857–864. doi:10.1016/j.jvir.2011.01.458.

Hall, E. L. (1974). Almost uniform distributions for computer image enhancement. *IEEE Transactions on Computers, 100*(2), 207–208. doi:10.1109/T-C.1974.223892.

Hashemi, S., Kiani, S., Noroozi, N., & Moghaddam, M. E. (2010). An image contrast enhancement method based on genetic algorithm. *Pattern Recognition Letters, 31*(13), 1816–1824. doi:10.1016/j.patrec.2009.12.006.

Holland, J. H. (1992). *Adaptation in natural and artificial systems: An introductory analysis with applications to biology, control and artificial intelligence*. Cambridge, MA, USA: MIT Press.

Karaboga, D., & Basturk, B. (2007). A powerful and efficient algorithm for numerical function optimization: Artificial bee colony (ABC) algorithm. *Journal of Global Optimization, 39*(3), 459–471. doi:10.1007/s10898-007-9149-x.

Kennedy, J., & Eberhart, R. (1995). Particle swarm optimization. In *Proceeding of the IEEE international conference on neural networks: 4* (pp. 1942–1948). doi:10.1109/ICNN.1995.488968.

Kim, Y. T. (1997). Contrast enhancement using brightness preserving bi-histogram equalization. *IEEE Transactions on Consumer Electronics, 43*(1), 1–8. doi:10.1109/30.580378.

Kohmura, H., & Wakahara, T. (2006). Determining optimal filters for binarization of degraded characters in color using genetic algorithms. In *18th international conference on pattern recognition (ICPR 2006): 3* (pp. 661–664). IEEE. doi:10.1109/ICPR.2006.446.

Koza, J. R. (1992). *Genetic programming: On the programming of computers by means of natural selection* (1st). Cambridge, MA, USA: MIT Press.

Krupinski, E. A. (2010). Current perspectives in medical image perception. *Attention Perception & Psychophysics, 72*(5), 1205–1217. doi:10.3758/APP.72.5.1205.

Lambin, P., Leijenaar, R. T. H., Deist, T. M., Peerlings, J., de Jong, E. E. C., van Timmeren, J., et al. (2017). Radiomics: The bridge between medical imaging and personalized medicine. *Nature Reviews Clinical Oncology, 14*(12), 749–762. doi:10.1038/nrclinonc.2017.141.

Leksell, L. (1949). A stereotaxic apparatus for intracerebral surgery. *Acta Chirurgica Scandinavica, 99*, 229–233.

Meier, R., Knecht, U., Loosli, T., Bauer, S., Slotboom, J., Wiest, R., & Reyes, M. (2016). Clinical evaluation of a fully-automatic segmentation method for longitudinal brain tumor volumetry. *Scientific Reports, 6*. doi:10.1038/srep23376.

Meijering, E. (2012). Cell segmentation: 50 years down the road. *IEEE Signal Processing Magazine, 29*(5), 140–145. doi:10.1109/MSP.2012.2204190.

Metcalfe, P., Liney, G. P., Holloway, L., Walker, A., Barton, M., Delaney, G. P., et al. (2013). The potential for an enhanced role for MRI in radiation-therapy treatment planning. *Technology in Cancer Research & Treatment, 12*(5), 429–446. doi:10.7785/tcrt.2012.500342.

Militello, C., Rundo, L., & Gilardi, M. C. (2014). Applications of imaging processing to MRgfus treatment for fibroids: A review. *Translational Cancer Research, 3*(5), 472–482. doi:10.3978/j.issn.2218-676X.2014.09.06.

Militello, C., Rundo, L., Vitabile, S., Russo, G., Pisciotta, P., Marletta, F., et al. (2015a). Gamma knife treatment planning: MR brain tumor segmentation and volume measurement based on unsupervised fuzzy c-means clustering. *The International Journal of Imaging Systems and Technology, 25*(3), 213–225. doi:10.1002/ima.22139.

Militello, C., Vitabile, S., Rundo, L., Russo, G., Midiri, M., & Gilardi, M. C. (2015b). A fully automatic 2D segmentation method for uterine fibroid in MRgfus treatment evaluation. *Computers in Biology and Medicine, 62*, 277–292. doi:10.1016/j.compbiomed.2015.04.030.

Miller, B. L., & Goldberg, D. E. (1995). Genetic algorithms, tournament selection, and the effects of noise. *Complex Systems, 9*(3), 193–212.

Muangkote, N., Sunat, K., & Chiewchanwattana, S. (2017). R<sub>r-cr</sub>-IJADE: An efficient differential evolution algorithm for multilevel image thresholding. *Expert Systems with Applications, 90*, 272–289. doi:10.1016/j.eswa.2017.08.029.

Munteanu, C., & Rosa, A. (2004). Gray-scale image enhancement as an automatic process driven by evolution. *IEEE Transactions on Systems, Man, and Cybernetics, 34*(2), 1292–1298. doi:10.1109/TSMCB.2003.818533.

Ortiz, A., Górriz, J. M., Ramírez, J., Salas-Gonzalez, D., & Llamas-Elvira, J. M. (2013). Two fully-unsupervised methods for MR brain image segmentation using SOM-based strategies. *Applied Soft Computing, 13*(5), 2668–2682. doi:10.1016/j.asoc.2012.11.020.

Otsu, N. (1975). A threshold selection method from gray-level histograms. *IEEE Transactions on Systems, Man, and Cybernetics, 11*(285–296), 23–27. doi:10.1109/TSMC.1979.4310076.

Paranjape, R. B. (2009). Chapter 1- fundamental enhancement techniques. In I. N. Bankman (Ed.), *Handbook of Medical Image Processing and Analysis* (pp. 3–18). Burlington, MA, USA: Academic Press. doi:10.1016/B978-012373904-9.50008-8.

Paulinas, M., & Ušinskas, A. (2007). A survey of genetic algorithms applications for image enhancement and segmentation. *Information Technology and Control, 36*(3), 278–284.

Poli, R., & Cagnoni, S. (1997). Genetic programming with user-driven selection: experiments on the evolution of algorithms for image enhancement. In *2nd annual conference on genetic programming* (pp. 269–277).

Rajchl, M., Lee, M. C. H., Oktay, O., Kamnitsas, K., Passerat-Palmbach, J., Bai, W., et al. (2017). Deepcut: Object segmentation from bounding box annotations using convolutional neural networks. *IEEE Transactions on Medical Imaging, 36*(2), 674–683. doi:10.1109/TMI.2016.2621185.

Rangayyan, R. M. (2009). Part I- Enhancement. In I. N. Bankman (Ed.), *Handbook of Medical Image Processing and Analysis* (pp. 1–2). Burlington, MA, USA: Academic Press. doi:10.1016/B978-012373904-9.50008-8.

Ridler, T. W., & Calvard, S. (1978). Picture thresholding using an iterative selection method. *IEEE Transactions on Systems, Man, and Cybernetics, 8*(8), 630–632. doi:10.1109/TSMC.1978.4310039.

Rueckert, D., Glocker, B., & Kainz, B. (2016). Learning clinically useful information from images: past, present and future. *Medical Image Analysis, 33*, 13–18. doi:10.1016/j.media.2016.06.009.

Rundo, L., Militello, C., Tangherloni, A., Russo, G., Lagalla, R., Mauri, G., et al. (2019). Computer-assisted approaches for uterine fibroid segmentation in MRgfus treatments: Quantitative evaluation and clinical feasibility analysis. In *Quantifying and processing biomedical and behavioral signals*. In *Smart Innovation, Systems and Technologies: 103* (pp. 229–241). Springer. doi:10.1007/978-3-319-95095-2_22.

Rundo, L., Stefano, A., Militello, C., Russo, G., Sabini, M. G., D'Arrigo, C., et al. (2017). A fully automatic approach for multimodal PET and MR image segmentation in gamma knife treatment planning. *Computer Methods and Programs in Biomedicine, 144*, 77–96. doi:10.1016/j.cmpb.2017.03.011.

Saitoh, F. (1999). Image contrast enhancement using genetic algorithm. In *Proc. ieee international conference on systems, man, and cybernetics (smc): 4* (pp. 899–904). IEEE. doi:10.1109/ICSMC.1999.812529.

Scheuermann, T., & Hensley, J. (2007). Efficient histogram generation using scattering on GPUs. In *Proc. symposium on interactive 3D graphics and games* (pp. 33–37). ACM. doi:10.1145/1230100.1230105.

Shanmugavadivu, P., & Balasubramanian, K. (2014). Particle swarm optimized multi-objective histogram equalization for image enhancement. *Optics & Laser Technology, 57*, 243–251. doi:10.1016/j.optlastec.2013.07.013.

Singh, M., Verma, A., & Sharma, N. (2017). Bat optimization based neuron model of stochastic resonance for the enhancement of MR images. *Biocybernetics and Biomedical Engineering, 37*(1), 124–134. doi:10.1016/j.bbe.2016.10.006.

Sompong, C., & Wongthanavasu, S. (2017). An efficient brain tumor segmentation based on cellular automata and improved tumor-cut algorithm. *Expert Systems with Applications, 72*, 231–244. doi:10.1016/j.eswa.2016.10.064.

Sourbron, S. P., & Buckley, D. L. (2013). Classic models for dynamic contrast-enhanced MRI. *NMR in Biomedicine, 26*(8), 1004–1027. doi:10.1002/nbm.2940.

Starck, J. L., Murtagh, F., Candes, E. J., & Donoho, D. L. (2003). Gray and color image contrast enhancement by the curvelet transform. *IEEE Transactions on Image Processing, 12*(6), 706–717. doi:10.1109/TIP.2003.813140.

Styner, M., Brechbuhler, C., Széckely, G., & Gerig, G. (2000). Parametric estimate of intensity inhomogeneities applied to MRI. *IEEE Transactions on Medical Imaging, 19*(3), 153–165. doi:10.1109/42.845174.

Toennies, K. D. (2017). *Guide to medical image analysis* (3rd). London, UK: Springer-Verlag. doi:10.1007/978-1-4471-7320-5.

Trussell, H. J. (1979). Comments on picture thresholding using an iterative selection method. *IEEE Transactions on Systems, Man, and Cybernetics, 9*(5). doi:10.1109/TSMC.1979.4310204. 311–311

Wang, Z., & Bovik, A. C. (2002). A universal image quality index. *IEEE Signal Processing Letters, 9*(3), 81–84. doi:10.1109/97.995823.

Wang, Z., Bovik, A. C., Sheikh, H. R., & Simoncelli, E. P. (2004). Image quality assessment: From error visibility to structural similarity. *IEEE Transactions on Image Processing, 13*(4), 600–612. doi:10.1109/TIP.2003.819861.

Xue, J. H., & Zhang, Y. J. (2012). Ridler and calvard's, kittler and illingworth's and otsu's methods for image thresholding. *Pattern Recognition Letters, 33*(6), 793–797. doi:10.1016/j.patrec.2011.01.021.